On modeling micro-structural evolution using a higher order strain gradient continuum theory

El-Naaman, S. A.; Nielsen, K. L.; Niordson, C. F.

Published in:
International Journal of Plasticity

Link to article, DOI:
10.1016/j.ijplas.2015.08.008

Publication date:
2016

Document Version
Peer reviewed version

On modeling micro-structural evolution using a higher order strain gradient continuum theory

S.A. El-Naaman*, K.L. Nielsen, C.F. Niordson

Department of Mechanical Engineering, Solid Mechanics, Technical University of Denmark, DK-2800 Kgs. Lyngby, Denmark

Abstract

Published experimental measurements on deformed metal crystals show distinct pattern formation, in which dislocations are arranged in wall and cell structures. The distribution of dislocations is highly non-uniform, which produces discontinuities in the lattice rotations. Modeling the experimentally observed micro-structural behavior, within a framework based on continuous field quantities, poses obvious challenges, since the evolution of dislocation structures is inherently a discrete and discontinuous process. This challenge, in particular, motivates the present study, and the aim is to improve the micro-structural response predicted using strain gradient crystal plasticity within a continuum mechanics framework. One approach to modeling the dislocation structures observed is through a back stress formulation, which can be related directly to the strain gradient energy. The present work offers an investigation of constitutive equations for the back stress based on both considerations of the gradient energy, but also includes results obtained from a purely phenomenological starting point. The influence of model parameters is brought out in a parametric study, and it is demonstrated how a proper treatment of the back stress enables dislocation wall and cell structure

*Tel: +45 4525-4020, Fax: +45 4593-1475
URL: saeln@mek.dtu.dk (S.A. El-Naaman)

type response in the adopted framework.

Keywords: Strain gradient plasticity, Size-effects, Strain gradient energy, Geometrically necessary dislocations, Back stress formulation

1. Introduction

The ability to accurately predict the response and performance of ductile crystalline materials, on the micron scale and below, is crucial for example when modeling forming processes with thin metal films. In multiscale plasticity problems, it has been established that in the presence of large deformation gradients—invoking a population of geometrically necessary dislocations (GNDs) that becomes significant compared to the statistically stored dislocations—conventional plasticity theory breaks down and so-called higher order strain gradient plasticity theories are needed. While there is an ongoing discussion on whether size-effects result in strain gradient strengthening (delayed yield point) or strain gradient hardening, non-trivial size-effects are well recognized. Since the first gradient dependent theory appeared some 30 years ago, micromechanically based crystal plasticity models have been a highly active research subject and recent contributions include Hutchinson (2012); Öztop et al. (2012); van Beers et al. (2013); Klusemann and Yalçinkaya (2013); Niordson and Kysar (2014). Different families of higher order strain gradient plasticity theories have evolved, but a common feature for all is that they incorporate micro-structural boundary conditions, enabling constraints on plastic flow or associated field quantities, as opposed to the so-called lower order theories (e.g Bassani, 2001; Huang et al., 2004) for which unexpected strain localization behavior was pointed out by Niordson and Hutchinson (2003).

It is well known that dislocations arrange themselves in wall and cell structures,

within grains of crystalline materials, during plastic deformation. Bands of high dislocation density (dislocation walls) typically form webs enclosing regions of relatively low dislocation content (cell interiors). Ananthan et al. (1991) report on clear mesh like dislocation structures in cold rolled polycrystalline copper, while the studies of Huang and Winther (2007) and Hong et al. (2013) reveal details on dislocation structures and geometrically necessary boundaries in aluminum and copper specimens. Recently, Öztop (2011) performed high resolution electron backscatter diffraction (HR-EBSD) measurements on a nickle single crystal, subject to wedge indentation in an approximate two-dimensional plane strain deformation state. These measurements show highly nonuniform and discontinuous lattice rotations, which are linked directly to the existence of geometrically necessary dislocations (GNDs), revealing distinct dislocation wall and cell pattern formation. Details on the experimental methods employed by Öztop (2011) can also be found in Kysar et al. (2010) and Dahlberg et al. (2014), also showing highly localized GND structures.

A vast number of numerical studies on the evolution of dislocation structure exist in the literature, some concerned with discrete dislocations and molecular dynamics (Deshpande et al., 2003, 2005; Yaghoobi and Voyiadjis, 2014; Tarleton et al., 2015; Voyiadjis and Yaghoobi, 2015), while others take a continuum approach (Yefimov et al., 2004; Klusemann and Yalçinkaya, 2013; van Beers et al., 2013). GNDs accommodate the plastic strain gradients and thus, walls of GNDs are associated with high slip gradients occurring in a small region, and therefore also high second gradients of slip. Continuum models of the micro-structural evolution tend to show a much smoother GND field, than observed in reality. Complex physics governs the movement of dislocations

at the atomic scale, and linking it to the governing equations of a multi-scale continuum model, poses a considerable challenge. An obvious issue with modeling the evolution of dislocation structures, in terms of continuous field quantities, is that this physical phenomenon is inherently a discrete and discontinuous process. Recently, van Beers et al. (2013) studied the grain boundary interface mechanics using a micro-structurally based formulation within the gradient crystal plasticity framework developed by Evers et al. (2004) and Bayley et al. (2006). Here, wall formation type behavior was predicted at the grain boundaries. However, the micro-structural development was characterized by a rather smooth distribution of GNDs, which clearly demonstrates the challenge of representing the highly nonuniform response associated with dislocation wall and cell structures.

Higher order theories are often categorized into two branches: Work conjugate theories and Non-work conjugate theories. The work conjugate type formulations (e.g. Gurtin, 2002) make use of higher-order stress concepts as work conjugates to the strain/slip gradients, whereas the non-work conjugate type theories do not. The present study employs the non-work conjugate type theory proposed by Kuroda and Tvergaard (2006, 2008), which is a higher order extension of conventional crystal plasticity theory. Nemat-Nasser et al. (1998) suggested a straight forward extension of the widely used visco-plastic power law slip rate relation (Hutchinson, 1976; Peirce et al., 1983), so that the slip rate, $\dot{\gamma}$, on the α'th slip system is given by

$$\dot{\gamma}^{(\alpha)} = \dot{\gamma}_0 \mathrm{sgn}\left(\tau^{(\alpha)} - \tau_b^{(\alpha)}\right) \left(\frac{|\tau^{(\alpha)} - \tau_b^{(\alpha)}|}{g^{(\alpha)}}\right)^{1/m}, \tag{1}$$

where the superposed dot denotes material time derivative, $\dot{\gamma}_0$ is a reference slip rate, $\tau^{(\alpha)}$ is the Schmid stress (taken as the macroscopic Cauchy stress tensor resolved onto

the slip plane), $\tau_b^{(\alpha)}$ is a back stress, m is the rate hardening exponent, and $g^{(\alpha)}$ is the slip resistance. In Eq. (1), the conventional power law slip rate relation is gradient-enhanced by replacing the resolved shear stress, $\tau^{(\alpha)}$, with an effective resolved shear stress taken as the difference between the Schmid stress and a back stress; $\tau^{(\alpha)} - \tau_b^{(\alpha)}$ (Groma, 1997; Evers et al., 2004)[1]. The back stress, $\tau_b^{(\alpha)}$, is related directly to the gradients of the GND density (see Section 4), impeding the occurrence of slip at nonuniform pile-ups of GNDs. With this concept, the effective resolved shear stress is perceived as the driving force behind the movement of dislocations (Evers et al., 2004). This type of model can accommodate nonuniform distributions of $\dot{\gamma}^{(\alpha)}$ under a constant stress state, which is needed to give rise to GNDs.

The present study aims to expand the modeling capabilities of predicting micro-structural evolution using strain gradient single crystal plasticity and takes a continuum mechanics approach to the problem. The paper investigates constitutive equations for the back stress and offers a discussion on the underlying physical arguments. Finally, a phenomenological model formulation, for predicting the micro-structural evolution and plastic material response on the sub-micron level, is proposed.

The paper is structured as follows. The strain gradient plasticity model is described in Section 2 and the scope of the paper is outlined in Section 3. Following is the derivation of back stress relations in Section 4, including a series of results presented using a finite element method (FEM) implementation. The final concluding remarks are offered in Section 5.

[1]Note that for $\tau_b^{(\alpha)}$ equal to zero, Eq. (1) reduces to the conventional theory.

2. Strain gradient crystal plasticity model

The non-work conjugate higher order strain gradient plasticity theory formulated by Kuroda and Tvergaard (2006, 2008) is employed in the present study. The theory is of a higher order nature but does not rely on higher order stress concepts. The formulation builds on the framework of conventional crystal visco-plasticity theory, where a second set of differential equations is introduced for the evolution of the GND densities. Here, the GND densities appear directly as free field variables. The present study employs a small strain formulation, so that; $\dot{\varepsilon}_{ij} = \left(\dot{u}_{i,j} + \dot{u}_{j,i}\right)/2$, and an additive decomposition of the total strain rate is used, so that; $\dot{\varepsilon}_{ij} = \dot{\varepsilon}^{e}_{ij} + \dot{\varepsilon}^{p}_{ij}$, where the superscripts 'e' and 'p' denote the elastic and plastic parts, respectively. Plastic deformation occurs by the mechanism of crystallographic slip on the individual slip systems denoted α. Thus, the plastic strain rate is given in terms of the sliprate as

$$\dot{\varepsilon}^{p}_{ij} = \sum_{\alpha} \dot{\gamma}^{(\alpha)} P^{(\alpha)}_{ij}, \quad P^{(\alpha)}_{ij} = \frac{1}{2}\left(s^{(\alpha)}_{i} m^{(\alpha)}_{j} + m^{(\alpha)}_{i} s^{(\alpha)}_{j}\right), \tag{2}$$

where $s^{(\alpha)}_{i}$ and $m^{(\alpha)}_{i}$ are unit vectors specifying the slip direction and slip plane normal, respectively, and $P^{(\alpha)}_{ij}$ is the Schmid orientation tensor (see also Fig. 1b for a schematic definition). The slip rates follow the relation given in Eq. (1), and involves the back stresses, which are the main subject of the present study. The slip resistance $g^{(\alpha)}$ in Eq. (1) is taken to follow the hardening law

$$\dot{g}^{(\alpha)} = \sum_{\beta} h^{(\alpha\beta)} |\dot{\gamma}^{(\beta)}|, \quad g^{(\alpha)}|_{t=0} = \tau_0, \tag{3}$$

where the initial value of $g^{(\alpha)}$ is chosen as the initial critical resolved shear stress τ_0, $h^{(\alpha\beta)}$ are slip hardening moduli, in which the trace accounts for self hardening and the off-diagonal parts for latent hardening, and t is time. The governing equations of

the non-work conjugate formulation, are given by the conventional stress equilibrium equation; $\sigma_{ij,j} + f_i = 0$, where f_i are body forces and the Cauchy stress rate is given by the elastic relationship; $\dot{\sigma}_{ij} = \mathscr{L}_{ijkl}\left(\dot{\varepsilon}_{kl} - \dot{\varepsilon}^p_{kl}\right)$, in which $\mathscr{L}_{ijkl}$ is the fourth order elastic stiffness tensor.

In the framework adopted, the gradients of GND densities influence the viscous slip rate through the back stress, which counteracts the resolved shear stress on the slip systems, and thus the plastic strain rate. This gives rise to a kinematic hardening contribution. In order to determine the distribution of GNDs, an additional set of differential equations is introduced, ensuring that the slip exists in balance with the GND densities:

$$\frac{1}{b}\gamma^{(\alpha)}_{,i} s^{(\alpha)}_i + \rho^{(\alpha)}_{G(e)} = 0 \tag{4a}$$

$$\frac{1}{b}\gamma^{(\alpha)}_{,i} p^{(\alpha)}_i + \rho^{(\alpha)}_{G(s)} = 0. \tag{4b}$$

Here, $\mathbf{p}^{(\alpha)} = \mathbf{s}^{(\alpha)} \times \mathbf{m}^{(\alpha)}$, b is the magnitude of the Burgers vector, and $\rho^{(\alpha)}_G$ are GND densities on slip system α, where the subscripts (e) and (s) denote edge and screw components, respectively (Ashby, 1970). The governing equations for the displacement field and GND density field are evaluated separately, however, the two fields are linked together by the back stress. Hence, it is through the back stress that the gradient effects influence the conventional field equations. Through the principle of virtual work, the weak form of the displacement field equation reads:

$$\int_V \mathscr{L}_{ijkl}\dot{\varepsilon}_{kl}\delta\dot{\varepsilon}_{ij}\mathrm{d}V = \int_V \mathscr{L}_{ijkl}\dot{\varepsilon}^p_{kl}\delta\dot{\varepsilon}_{ij}\mathrm{d}V + \int_V \dot{f}_i\delta\dot{u}_i\mathrm{d}V + \int_S \dot{T}_i\delta\dot{u}_i\mathrm{d}S, \quad \dot{T}_i \equiv \dot{\sigma}_{ij}n_j, \tag{5}$$

where $\dot{T}_i$ are the traction rates, n_i is the outward unit normal field of the surface S

bounding the volume V. The weak form of the GND density equations (4) read:

$$\frac{1}{b}\int_V \delta\rho_{,i} s_i^{(\alpha)} \gamma^{(\alpha)} \mathrm{d}V = \frac{1}{b}\int_S \delta\rho \zeta^{(\alpha)} \mathrm{d}S + \int_V \delta\rho \rho_{G(e)}^{(\alpha)} \mathrm{d}V, \qquad \zeta^{(\alpha)} \equiv \gamma^{(\alpha)} n_i s_i^{(\alpha)}, \tag{6a}$$

$$\frac{1}{b}\int_V \delta\rho_{,i} p_i^{(\alpha)} \gamma^{(\alpha)} \mathrm{d}V = \frac{1}{b}\int_S \delta\rho \eta^{(\alpha)} \mathrm{d}S + \int_V \delta\rho \rho_{G(s)}^{(\alpha)} \mathrm{d}V, \qquad \eta^{(\alpha)} \equiv \gamma^{(\alpha)} n_i p_i^{(\alpha)}, \tag{6b}$$

where $\delta\rho$ is a weighting function or virtual GND density. In the GND density equations, a hard interface impenetrable for dislocations can be enforced as

$$\zeta^{(\alpha)} \equiv \gamma^{(\alpha)} n_i s_i^{(\alpha)} = 0 \tag{7a}$$

$$\eta^{(\alpha)} \equiv \gamma^{(\alpha)} n_i p_i^{(\alpha)} = 0, \tag{7b}$$

whereas a free boundary, where dislocations are free to exit the domain, corresponds to

$$\rho_{G(e)}^{(\alpha)} = \rho_{G(s)}^{(\alpha)} = 0. \tag{8}$$

For a detailed discussion on the micro-structural boundary conditions see Kuroda and Tvergaard (2008).

3. Problem description

In the present study, the focus is on the micro-structural response in strain gradient crystal plasticity and an attempt is made to phenomenologically bridge the gap between the length scales. Traditionally, in strain gradient plasticity models, one can manipulate the material length scale parameter to capture size-effects, however, this does not necessarily lead to a realistic distribution of GNDs. In fact, current theories predict smooth and uniform micro-structures, which is not sufficient for describing the highly non-uniform nature of dislocation patterning. Generally, the clustering of dislocations is characterized by sharp and abrupt transitions between cell walls and cell interiors,

which, in a continuum context, translates into high spatial gradients of GND density. As will be demonstrated in the following section, the micro-structural behavior can be tied to the choice of free energy formulation and ultimately to the form of the back stress.

In order to quantify the desired response, in terms of dislocation wall and cell structures, it has been chosen to define a dislocation cell, within a phenomenological continuum mechanics representation, by the following two characteristics:

1 Dislocation wall: The minor portion of the cell structure, dominated by high GND density and high GND density gradients.

2 Cell interior: The major portion of the cell structure, dominated by low (several orders of magnitude lower than the walls) to zero GND density and low (approaching zero) GND density gradients.

The present study is confined to two dimensional space, i.e., all terms associated with screw dislocations vanish and the interaction between slip systems is omitted for clarity of the analysis. Thus, the single slip simple shear problem, illustrated in Fig. 1, is considered in order to demonstrate the influence of back stress formulations. In order to allow comparison with the results of Kuroda and Tvergaard (2008), the following model parameters are used throughout: Slip angle $\theta = 90^\circ$, Young's modulus $E = 130$ GPa, Poisson's ratio $\nu = 0.3$, $\tau_0 = 50$ MPa, $b = 0.286$ nm, $h^{(\alpha\beta)} = h = 250$ MPa, and $m = 0.02$. On the semi-infinite material slab, of height H and width W, the following

boundary conditions are imposed on the displacement field

$$u_1 = u_2 = 0 \ \text{ at } \ x_2 = 0 \tag{9a}$$

$$u_1 = U(t) = H\dot{\gamma}_0 t \ \text{ and } \ u_2 = 0 \ \text{ at } \ x_2 = H, \tag{9b}$$

where the overall macroscopic shear strain applied is $\Gamma = 0.03$. Microscopic clamped boundary conditions are imposed on the GND density field as

$$\zeta^{(\alpha)} \equiv \gamma^{(\alpha)} n_i s_i^{(\alpha)} = 0 \ \text{ at } \ x_2 = 0 \ \text{ and } \ x_2 = H, \tag{10}$$

and periodicity in the x_1-direction requires that

$$u_i(0, x_2) \quad = u_i(W, x_2) \tag{11a}$$

$$\rho^{(\alpha)}_{G(e)}(0, x_2) = \rho^{(\alpha)}_{G(e)}(W, x_2). \tag{11b}$$

This means that all fields become effectively one dimensional. The results are obtained using the finite element method (FEM), solving the conventional system of equations and the GND system of equations in a staggered scheme. The discretized finite element equations can be found in Kuroda and Tvergaard (2008). Eight-node isoparametric quadrilateral elements with reduced Gauss integration are used for the displacement field analysis, whereas equivalent four-node elements with full Gauss integration are used for the GND density field analysis. Time integration is done by the forward Euler method. Typical finite element meshes consist of 50 elements in the x_2-direction and mesh refinements is used when steep gradients appear in the solution.

4. Back stress formulations and results

In the gradient visco-plasticity theory proposed by Kuroda and Tvergaard (2006, 2008), which is adopted in the present study, the back stress, τ_b, was originally assumed to

be proportional to the first gradients of the GND densities. When assuming that the back stress is given by the divergence of a vector-valued quantity higher order stress, $\xi_i^{(\alpha)}$;

$$\tau_b^{(\alpha)} \equiv -\xi_{i,i}^{(\alpha)}, \tag{12}$$

the adopted theory corresponds to the work conjugate theory of Gurtin (2000, 2002) through the micro-force balance equation

$$\xi_{i,i}^{(\alpha)} + \tau^{(\alpha)} - \tau_{eff}^{(\alpha)} = 0, \tag{13}$$

where $\tau_{eff}^{(\alpha)}$ is the effective resolved shear stress (given by $\tau_{eff}^{(\alpha)} = \tau^{(\alpha)} - \tau_b^{(\alpha)}$). The higher order stress, known as the work conjugate to the slip gradients in other theories, is derived from the free energy as

$$\xi_i^{(\alpha)} = \frac{\partial \psi_G^{(\alpha)}}{\partial \gamma_{,i}^{(\alpha)}}, \tag{14}$$

where ψ_G is the plastic part of the free energy, which is associated with slip gradients. Using relation (12), the non-work conjugate theory is rewritten in a work conjugate form. Following this framework in the model development ensures that it automatically comes out in a thermodynamically consistent manner, once a constitutive relation for the gradient energy, ψ_G, has been assumed. The gradient energy is often taken to be of a quadratic nature on the form (see e.g. Kuroda and Tvergaard, 2006, 2008; Anand et al., 2012; Klusemann and Yalçinkaya, 2013; Niordson and Kysar, 2014)

$$\psi_G^{(\alpha)} = \frac{1}{2}\tau_0 L^2 \left(\gamma_{,i}^{(\alpha)} s_i^{(\alpha)}\right)^2, \tag{15}$$

where L is a material length scale parameter, entering for dimensional consistency. This form of the gradient energy, however, is chosen primarily for mathematical convenience

rather than based on physical arguments. Assuming the quadratic gradient energy in Eq. (15), the Eqs. (12) and (14) lead to the following back stress relation, depending on the second gradients of slip

$$\tau_b^{(\alpha)} = -\tau_0 L^2 \gamma_{,ij}^{(\alpha)} s_i^{(\alpha)} s_j^{(\alpha)}, \tag{16}$$

which, expressed in terms of GND densities, becomes

$$\tau_b^{(\alpha)} = b\tau_0 L^2 \rho_{G(e),i}^{(\alpha)} s_i^{(\alpha)}. \tag{17}$$

While this theory captures size effects in strain gradient hardening well, it cannot capture, realistically, the highly non-uniform dislocation structures observed in experimental studies of e.g. wedge indentation (Kysar et al., 2010; Öztop, 2011; Dahlberg et al., 2014). The single slip simple shear problem, described in Section 3 and Fig. 1, is solved to demonstrate the behavior of the model assuming the classical perception of the back stress. Results for different values of the material length scale parameter, L, are shown in Fig. 2, assuming a quadratic gradient energy and thus the back stress in Eqs. (16) and (17). The slip profile across the material slab is shown in Fig. 2a and the GND profile is shown in Fig. 2b. The slip profile indicates an increasing flattening of the central part for decreasing L, while a rather smooth distribution of GNDs is obtained. It is noticed, however, that increased localization of GNDs takes place at the boundaries for decreasing values of L. The shear stress vs. macroscopic shear strain response is shown in Fig. 2c. Hardening clearly increases with L, as the back stress effect becomes increasingly significant, whereas for very low values of L, the size-effect diminishes. Similar results can be found in Anand et al. (2005). Although no experimental results exist for direct comparison with the plane strain simple shear

case, this boundary value problem outlines the model's ability to represent the highly localized GND structures observed experimentally[2].

It is possible to achieve increasingly non-uniform GND density distributions, when decreasing the influence of L, however, decreasing L until a satisfactory micro-structure is achieved clearly does not guarantee the proper size-dependence in the hardening behavior. Thus, in general one must assume that more than one constitutive parameter is needed for a model describing both size-effects and evolution of micro-structure.

In the following, alternative options for the back stress formulation will be explored in order to pursue a GND field response closer to experimental observations. There are arguments pointing toward a gradient energy which is closer to linear rather than quadratic (Evans and Hutchinson, 2009, see Section 5). A free energy potential linear in the slip gradients was investigated by Ohno and Okumara (2007) and Forest and Guéninchault (2013). Here, a generalization from the quadratic form of the gradient energy in Eq. (15), shall serve as basis for the following analysis. Assuming power law dependence on the slip gradients, one could write the gradient energy as

$$\psi_G^{(\alpha)} = \frac{1}{\mu+1}\tau_0 L^{\mu+1}\left|\gamma_{,i}^{(\alpha)} s_i^{(\alpha)}\right|^{\mu+1}. \tag{18}$$

A similar energy relation was proposed by Fredriksson and Gudmundson (2007) for interface modeling, where a near linear to quadratic dependence on the plastic strain was investigated. For a linear dependence on the plastic strain, their theory conforms with the dislocation based theory of Read and Shockley (1950) for low angle tilt boundaries.

[2]Moreover, in the wedge indentation case studied by Kysar et al. (2010), Öztop (2011), and Dahlberg et al. (2014), there are regions beneath the indentation which are dominated by approximate simple shear, of which Fig. 1 can be considered a simple model.

Recently, Bardella (2010), Bardella and Panteghini (2015), and Fleck et al. (2015) also proposed expressions for the free energy similar to Eq. (18). The generalized energy expression (Eq. (18)) leads to a back stress which is still a linear function of the second gradients of slip (as Eq. (17)), but in turn reveals a dependence on the first gradients of slip (or the GND densities), to the power of μ-1:

$$\tau_b^{(\alpha)} = -\mu\tau_0 L^{\mu+1} \left|\gamma_{,j}^{(\alpha)} s_j^{(\alpha)}\right|^{\mu-1} \gamma_{,ki}^{(\alpha)} s_i^{(\alpha)} s_k^{(\alpha)}, \tag{19}$$

which, expressed in terms of GND densities, becomes

$$\tau_b^{(\alpha)} = \mu\tau_0 b^{\mu} L^{\mu+1} \left|\rho_{G(e)}^{(\alpha)}\right|^{\mu-1} \rho_{G(e),i}^{(\alpha)} s_i^{(\alpha)}. \tag{20}$$

For $\mu = 1$, Eq. (18) is quadratic and Eqs. (19) and (20) reduce to Eqs. (16) and (17), respectively. The effect of μ is schematically illustrated in Fig. 3. In the studies by Groma et al. (2003) and Yefimov et al. (2004) on a single slip continuum description of dislocation dynamics, a back stress relation similar to Eq. (20) for $\mu \longrightarrow 0$ was found, based on the shear stress field of a single dislocation. In fact, the functional dependence on dislocation densities in Yefimov et al. (2004) is identical to Eq. (20), if no distinction is made between the so-called total and signed dislocation densities (see Yefimov et al. (2004) Eq. 13). When the order of the gradient energy is lower than quadratic ($\mu < 1$), numerical solution becomes cumbersome, since the back stress then approaches infinity when the GND density approaches zero. Hence, with a combination of low GND density and relatively high GND density gradients, the numerical solution can become unstable. Therefore, for values of μ below one, an "effective" GND density $\rho_{G(e),eff}^{(\alpha)} = \left|\rho_{G(e)}^{(\alpha)}\right| + \rho_{G(e),0}$ replaces $\left|\rho_{G(e)}^{(\alpha)}\right|$ in Eq. (20), in order to exclude the effect of the singularity in the back stress function. A value of $\rho_{G(e),0} = 10^5$ m^{-2} is used in

the present computations and a sensitivity analysis showed $\rho_{G(e),0}$ to have negligible effect on the qualitative results. The effect of $\rho_{G(e),0}$ is demonstrated in Appendix A. The implications of the generalized back stress is demonstrated in Figs. 4 through 6. Figures 4 and 5 are equivalent but show results for two different regimes of the energy exponent, μ: Quadratic to cubic gradient energy ($1 \leq \mu \leq 2$) and nearly linear to quadratic gradient energy ($0 < \mu \leq 1$), respectively. From a phenomenological point of view, Fig. 4 shows interesting results. The flattening of the slip profile is seen for increasing values of μ in Fig. 4a, associated with an intense build-up of GND density at the boundaries (Fig. 4b). In the case of $\mu = 2$ (cubic energy), the GND density gradients are practically eliminated in the interior region of approximately 70 percent of the slab height, whereas a steep increase takes place at the boundaries. The GND density profile is normalized with its boundary value (the maximum GND density in the material domain, $\rho^{(1)}_{G(e),max}$) in order to qualitatively demonstrate the effect of μ. The normalization value, $\rho^{(1)}_{G(e),max}$, can be seen in Fig. 6 as function of μ. Here, the effect of μ is demonstrated for different values of the material length scale parameter, at a macroscopic strain level of $\Gamma = 0.03$. In the shear stress vs. macroscopic shear strain response (Fig. 4c), the linear hardening decreases with increasing μ. This is further demonstrated in Fig. 7 for different values of the material length scale parameter. Figure 5 shows results in the linear to quadratic regime of the gradient energy, with the flattening of the slip profile evident for low values of μ (Fig. 5a). As μ goes to one, the effect of the back stress singularity moves closer to $\rho_{G(e),0}$ and it starts to have an effect on the hardening behavior. This is seen, in Fig. 5a, as a small notch on the slip profile in the center region of the material domain, that diminishes as μ

goes to zero. Figure 5b shows the GND density profile, where the density is found to intensify at the boundaries for very low values of μ, however, the opposite effect occurs at intermediate values, e.g. at $\mu = 0.4$. The general trend of the dependence on μ has a turning point, which appears as a local minimum in Fig. 6, when plotting $\rho^{(1)}_{G(e),max}$ as function of μ. The local minimum shifts upward for increasing L and is seen, e.g., at approximately $\mu = 0.5$ for $L/H = 0.3$. Figure 5c shows the shear stress vs. macroscopic shear strain, where a non-linear response is observed for lower values of μ. Here, as well, a non-trivial effect of μ is predicted, which is evident from Fig. 7. It is seen that the flow stress level at $\Gamma = 0.03$ has a local maximum, which shifts upward for increasing L. This maximum is found, e.g., at approximately $\mu = 0.3$ for $L/H = 0.3$ (see Fig. 7).

Evers et al. (2004) argue that the GND density itself does not contribute to the long range internal stresses (i.e. the back stress). However, this is not the case in Eq. (20), where a strong dependence on the GND density is seen. The authors do not attempt to advocate any physical advantages of the dependence on GND density, however, it is noted that a uniform GND field yields zero back stress in accordance with the arguments put forth by Evers et al. (2004).

When $\mu \longrightarrow 0$ or $\mu \longrightarrow 2$ in the back stress relation in Eqs. (19) and (20), slip localization is promoted through its relationship with the GND density, enabling GND wall formation at the hard boundaries. This type of behavior can also be imposed through the relationship between the back stress and the GND density gradients, since a GND wall is also tied to high levels of GND density gradients. In the framework proposed by Kuroda and Tvergaard (2006, 2008) any function $\tau_b^{(\alpha)}\left(\rho^{(\alpha)}_{G(e),i} s_i^{(\alpha)}\right)$ may

be considered. Thus, one could assume the following power law proportionality for the back stress relation:

$$\tau_b^{(\alpha)} \propto \left| \rho_{G(e),i}^{(\alpha)} s_i^{(\alpha)} \right|^{\kappa}, \quad 0 \leq \kappa \leq 1. \tag{21}$$

For values of κ below one, this type of relation allows the slip to build up more severely with less restriction imposed by the back stress as the GND density gradients evolve. However, Eq. (21) has an initially infinite slope in the limit of $\kappa = 0$, which would cause numerical difficulties for low values of the quantity $\rho_{G(e),i}^{(\alpha)} s_i^{(\alpha)}$. Thus, in order to investigate the influence of $\left| \rho_{G(e),i}^{(\alpha)} s_i^{(\alpha)} \right|^{\kappa}$ in the back stress formulation, the quadratic gradient energy based back stress is taken as starting point in the back stress power law, so that

$$\tau_b^{(\alpha)} = \begin{cases} b\tau_0 L^2 \rho_{G(e),i}^{(\alpha)} s_i^{(\alpha)} & , \text{ for } \tau_b^{(\alpha)} \leq \tau_T \\ \operatorname{sgn}\left(\rho_{G(e),i}^{(\alpha)} s_i^{(\alpha)} \right) b^{\kappa} \tau_T^{1-\kappa} \tau_0^{\kappa} L^{2\kappa} \left| \rho_{G(e),i}^{(\alpha)} s_i^{(\alpha)} \right|^{\kappa} & , \text{ for } \tau_b^{(\alpha)} > \tau_T \end{cases}, \tag{22}$$

with τ_T being a transition back stress parameter. When κ is equal to one, Eq. (22) reduces to the expression in Eq. (17), i.e., corresponding to a quadratic gradient energy. With κ equal to zero, Eq. (22) corresponds to a blunt cut-off of the back stress at $\tau_b^{(\alpha)} = \tau_T$. A schematic representation of this back stress relation can be found in Fig. 8. This set-up allows for the back stress to build up linearly, with the gradients of GND density, to a certain level before evolving according to a power law. The two formulations (Eqs. (20) and (22)) coincide for μ and κ equal to one (quadratic gradient energy), for which the back stress in Eq. (22) naturally provides a thermodynamically consistent theory. However, since the full back stress power law in Eq. (22) does not originate from a gradient energy constitutive law, the general form of Eq. (22) must be considered a non-thermodynamically consistent formulation. Figure 9 shows results

using the back stress power law relation in Eq. (22) for different values of κ with $\tau_T/\tau_0 = 0.12$ and $L/H = 0.3$. Figure 9a shows the slip profile with increased localized slip at the boundaries for decreasing values of κ and Fig. 9b shows the GND density profile normalized with the value at the boundary, $\rho^{(1)}_{G(e),max}$, in order to qualitatively demonstrate the effect of κ. Here, the transition point, $\tau_b = \tau_T$, is marked with a small circle on the individual curves near the lower boundary for the values $0 < \kappa < 1$. This point appears exactly on the boundary for κ equal to zero, since in this case the back stress is forced to not exceed τ_T (hence, not marked on the figure). The normalization value is presented in Fig. 10 as function of κ, showing also the effect of the material length scale parameter L. Here, it is noticed that the effect of L, on the level of GND density at the boundaries, changes character in the low regime of κ. As κ approaches zero, the GNDs evolve more locally, whereby more pronounced dislocation "walls" form. Thus, for low values of κ, the micro-structural response bears closer resemblance to what is observed in experimental studies. The results demonstrate that a highly non-uniform micro-structure, with high GND density at the boundaries and low GND density and GND density gradients in the interior region, can be achieved through the dependence of the back stress on the GND density gradient. Figure 9c shows the shear stress vs. macroscopic shear strain response with little effect of the κ parameter—though with a slight non-linear hardening effect appearing as κ decreases. The effect of κ on the flow stress is further demonstrated in Fig. 11 for different values of the material length scale. The effect of the rate exponent, m, on the GND density distribution, using back stress relation (22), was studied in El-Naaman et al. (2015), where increasing values of m was shown to increase the effect of κ.

5. Concluding remarks

A finite element implementation of the non-work conjugate higher order strain gradient crystal plasticity model, proposed by Kuroda and Tvergaard (2006, 2008), has formed the basis in the development of back stress formulations aimed at improving the ability to predict micro-structural evolution. This paper treats the highly idealized pure shear case, which serves as a benchmark for the performance of the proposed model.

Motivated by experimental observations, two distinct back stress formulations have been proposed in the present study:

i) A back stress based on a general formulation of the strain gradient energy, which provides a thermodynamically consistent theory (Eqs. (19) and (20)). This formulation ensures that the GND density field develops more localized and intensely for a gradient energy in the near linear regime but also in the high quadratic to cubic regime. Thereby, two alternatives are revealed, in terms of the exponential order of the gradient energy, improving the micro-structural response and enabling the representation of a dislocation wall and cell structure. This finding partly supports the argument put forth by Evans and Hutchinson (2009), that the energy associated with GNDs is likely linearly dependent on the plastic strain gradient.

ii) A purely phenomenologically devised back stress power law formulation, taking as starting point the quadratic form of the gradient energy. Here, an exponent κ on the gradients of the GND density, is introduced (see Eq. (22)). This formulation has no direct dependence on the GND density—in line with the quadratic energy based back stress in Eq. (17). Low values of the exponent κ produce a steeper

build up of the GND density at the micro-structurally passivated boundaries. Thus, a dislocation wall and cell type response can be achieved through the additional constitutive parameter κ.

With the two different formulations, summarized above, it has been shown that it is possible to achieve a micro-structural response that can represent a dislocation wall and cell structure (as defined in Section 3), while preserving the possibility of capturing size-effects. This feature, which a quadratic gradient energy derived back stress excludes, is offered in the proposed formulations through the introduction of an additional constitutive parameter, dedicated to calibrating the model against experimentally observed micro-structures.

Further research on more complicated boundary value problems, e.g. including multi-slip and latent hardening, as well as an investigation of the proposed models' performance under cyclic loading, is needed in order to fully establish their capabilities.

6. Acknowledgements

The work is financially supported by The Danish Council for Independent Research under the research career programme Sapere Aude in the project "Higher Order Theories in Solid Mechanics", grant 11-105098/FTP.

References

Anand, L., Aslan, O., Chester, S., 2012. A large-deformation gradient theory for elastic-plastic materials: Strain softening and regularization of shear bands. International Journal of Plasticity 30-31, 116–143.

Anand, L., Gurtin, M., Lele, S., Gething, C., 2005. A one-dimensional theory of strain-gradient plasticity: Formulation, analysis, numerical results. Journal of the Mechanics and Physics of Solids 53, 1789–1826.

Ananthan, V., Leffers, T., Hansen, N., 1991. Cell and band structures in cold-rolled polycrystalline copper. MATERIALS SCIENCE AND TECHNOLOGY 7, 1069–1075.

Ashby, M., 1970. The deformation of plastically non-homogeneous alloys. Philos. Mag. 21, 399–424.

Bardella, L., 2010. Size effects in phenomenological strain gradient plasticity constitutively involving the plastic spin. International Journal of Engineering Science 48, 550–568.

Bardella, L., Panteghini, A., 2015. Modelling the torsion of thin metal wires by distortion gradient plasticity. Journal of the Mechanics and Physics of Solids 78, 467–492.

Bassani, J., 2001. Incompressibility and a simple gradient theory of plasticity. Journal of the Mechanics and Physics of Solids 49, 1983–1996.

Bayley, C., Brekelmans, W., Geers, M., 2006. A comparison of dislocation induced back stress formulations in strain gradient crystal plasticty. International Journal of Solids and Structures 43, 7268–7286.

Dahlberg, C., Saito, Y., Öztop, M., Kysar, J., 2014. Geometrically necessary dislocation density measurements associated with different angles of indentations. International Journal of Plasticity 54, 81–95.

Deshpande, V., Needleman, A., Van der Giessen, E., 2003. Finite strain discrete dislocation plasticity. Journal of the Mechanics and Physics of Solids 51, 2057–2083.

Deshpande, V., Needleman, A., Van der Giessen, E., 2005. Plasticity size effects in tension and compression of single crystals. Journal of the Mechanics and Physics of Solids 53, 2661–2691.

El-Naaman, S., Nielsen, K., Niordson, C., 2015. Strain gradient crystal plasticity: A continuum mechanics approach to modeling micro-structural evolution. Plastic Behavior of Conventional and Advanced Materials: Theory, Experiment, and Modeling, 7–9.

Evans, A., Hutchinson, J., 2009. A critical assessment of theories of strain gradient plasticity. Acta Materialia 57, 1675–1688.

Evers, L., Brekelmans, W., Geers, M., 2004. Non-local cystal plasticity model with intrinsic SSD and GND effects. Journal of the Mechanics and Physics of Solids 52, 2379–2401.

Fleck, N., Hutchinson, J., Willis, J., 2015. Guidelines for constructing strain gradient plasticity theories. Journal of Applied Mechanics 82, 1–10.

Forest, S., Guéninchault, N., 2013. Inspection of free energy functions in gradient crystal plasticity. Acta Mechanica Sinica 29(6), 763–772.

Fredriksson, P., Gudmundson, P., 2007. Modelling of the interface between a thin film and a substrate within a strain gradient plasticity framework. Journal of the Mechanics and Physics of Solids 55 (5), 939 – 955.

Groma, I., 1997. Link between the microscopic and mesoscopic length-scale description of the collective behavior of dislocations. Physical Review B 56 (10).

Groma, I., Csikor, F., Zaizer, M., 2003. Spatial correlations and higher-order gradient terms in a continuum description of dislocation dynamics. Acta Materialia 51, 1271–1281.

Gurtin, M., 2000. On the plasticity of single crystals: free energy, microforces, plastic-strain gradients. Journal of the Mechanics and Physics of Solids 48 (5), 989–1036.

Gurtin, M., 2002. A gradient theory of single-crystal viscoplasticity that accounts for geometrically necessary dislocations. Journal of the Mechanics and Physics of Solids 50, 5–32.

Hong, C., Huang, X., Winter, G., 2013. Dislocation content of geometrically necessary boundaries aligned with slip planes in rolled aluminium. Philosophical Magazine 93 (23), 3118–3141.

Huang, X., Winther, G., 2007. Dislocation structures. Part I. Grain orientation dependence. Philosophical Magazine 87 (33), 5189–5214.

Huang, Y., Qu, S., Hwang, K., Li, M., Gao, H., 2004. A conventional theory of mechanism-based strain gradient plasticity. International Journal of Plasticity 20, 753–782.

Hutchinson, J., 1976. Bounds and self-consistent estimates for creep of polycrystalline materials. Proc. R. Soc. Lond. A 348, 101–127.

Hutchinson, J., 2012. Generalized J_2 flow theory: Fundamental issues in strain gradient plasticity. Acta Mechanica Sinica 28(4), 1078–1086.

Klusemann, B., Yalçinkaya, T., 2013. Plastic deformation induced microstructure evolution through gradient enhanced crystal plasticity based on a non-convex Helmholtz energy. International Journal of Plasticity 48, 168–188.

Kuroda, M., Tvergaard, V., 2006. Studies of scale dependent crystal viscoplasticity models. Journal of the Mechanics and Physics of Solids 54, 1789–1810.

Kuroda, M., Tvergaard, V., 2008. On the formulation of higher-order strain gradient crystal plasticity models. Journal of the Mechanics and Physics of Solids 56, 1591–1608.

Kysar, J., Saito, Y., Oztop, M., Lee, D., Huh, W., 2010. Experimental lower bounds on geometrically necessary dislocation density. International Journal of Plasticity 26, 1097–1123.

Nemat-Nasser, S., Luqun, N., Okinaka, T., 1998. A constitutive model for fcc crystals with application to polycrystalline OFHC copper. Mechanics of Materials 30, 325–341.

Niordson, C., Hutchinson, J., 2003. On lower order strain gradient plasticity theories. European Journal of Mechanics A/Solids 22, 771–778.

Niordson, C., Kysar, J., 2014. Computational strain gradient crystal plasticity. Journal of the Mechanics and Physics of Solids 62, 31–47.

Ohno, N., Okumara, D., 2007. Higher-order stress and grain size effects due to self-energy of geometrically necessary dislocations. Journal of the Mechanics and Physics of Solids 55, 1879–1898.

Öztop, M., 2011. Multiscale experimental analysis in plasticity: Linking dislocation structures to continuum fields. Ph.D. thesis, Columbia University.

Öztop, M., Niordson, C., Kysar, J., 2012. Length-scale effect due to periodic variation of geometrically nescessary dislocaion densities. International Journal of Plasticity 41, 189–201.

Peirce, D., Asaro, R., Needleman, A., 1983. Material rate dependence and localized deformation in crystalline solids. Acta Metall. 31, 1951–1976.

Read, W., Shockley, W., 1950. Dislocation models of crystal grain boundaries. Physical Review 78, 275–289.

Tarleton, E., Balint, D., Gong, J., Wilkinson, A., 2015. A discrete dislocation plasticity study of the micro-cantilever size effect. Acta Materialia 88, 271–282.

van Beers, P., McShane, G., Kouznetsova, V., Geers, M., 2013. Grain boundary interface mechanics in strain gradient crystal plasticity. Journal of the Mechanics and Physics of Solids 61, 2659–2679.

Voyiadjis, G., Yaghoobi, M., 2015. Large scale atomistic simulation of size effects during nanoindentation: Dislocation length and hardness. Materials Science & Engineering A 634, 20–31.

Yaghoobi, M., Voyiadjis, G., 2014. Effect of boundary conditions on the MD simulation of nanoindentation. Computational Materials Science 95, 626–636.

Yefimov, S., Groma, I., van der Giessen, E., 2004. A comparison of a statistical-mechanics based plasticity model with descrete dislocation plasticity calculations. Journal of the Mechanics and Physics of Solids 52, 279–300.

Figures

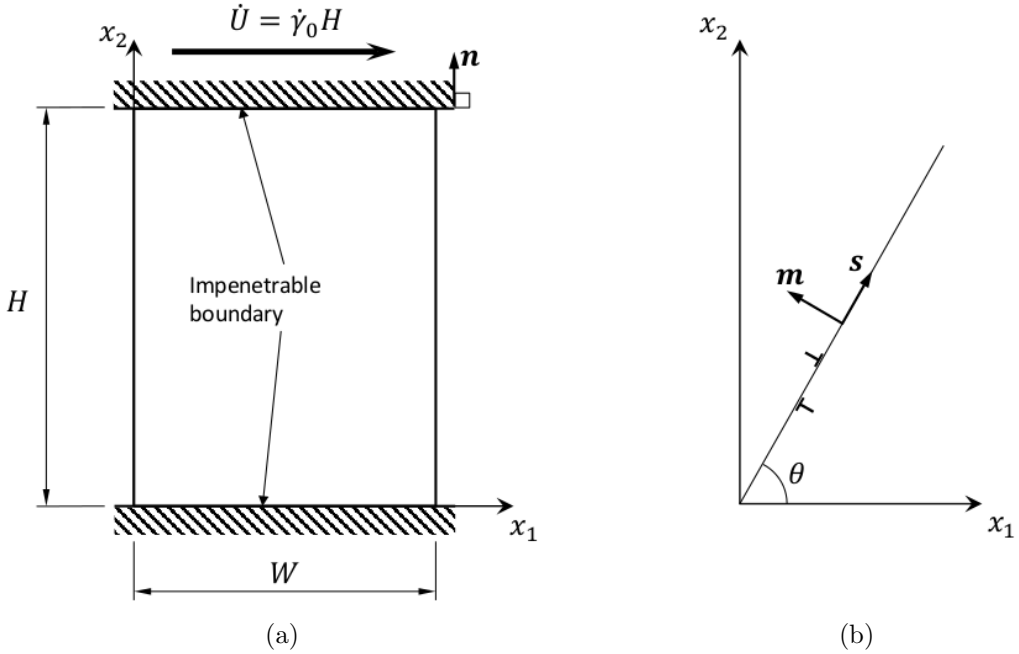

(a) (b)

Figure 1: Schematic of the simple shear problem: (a) a semi-infinite slab of material, constrained by two rigid impenetrable boundaries, subject to a prescribed displacement rate $\dot{U}$. (b) definition of the slip system.

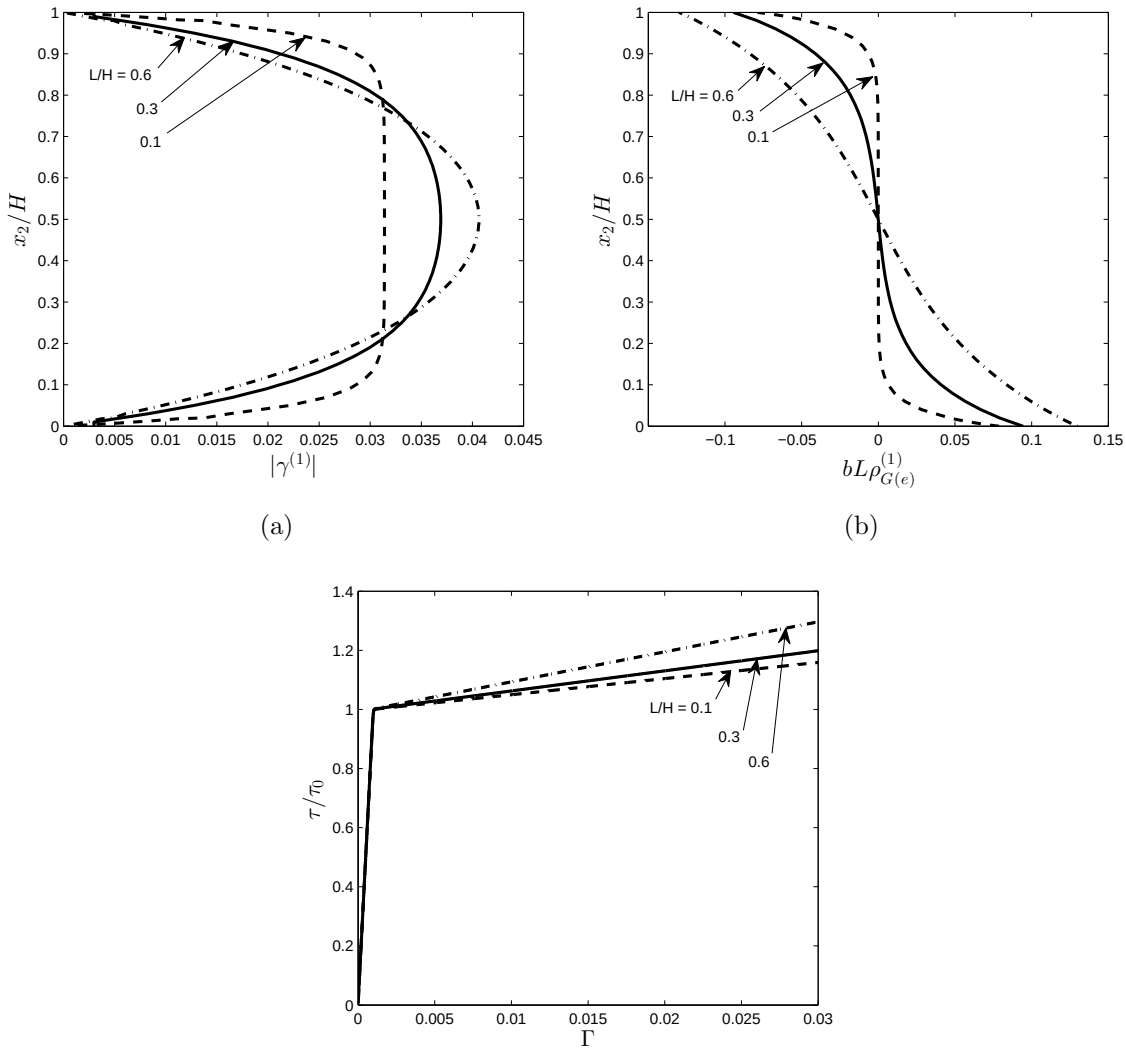

(a) (b)

(c)

Figure 2: Numerical results for the single slip simple shear problem (Fig. 1) with $\theta = 90°$, for different values of the material length scale parameter L. The figure shows (a) slip profile, (b) normalized GND density, and (c) shear stress vs. macroscopic shear strain.

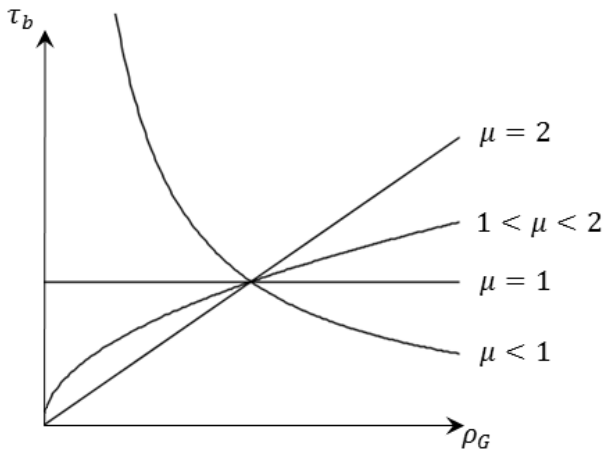

Figure 3: Schematic illustration of the generalized gradient energy based back stress law (Eq. (20)).

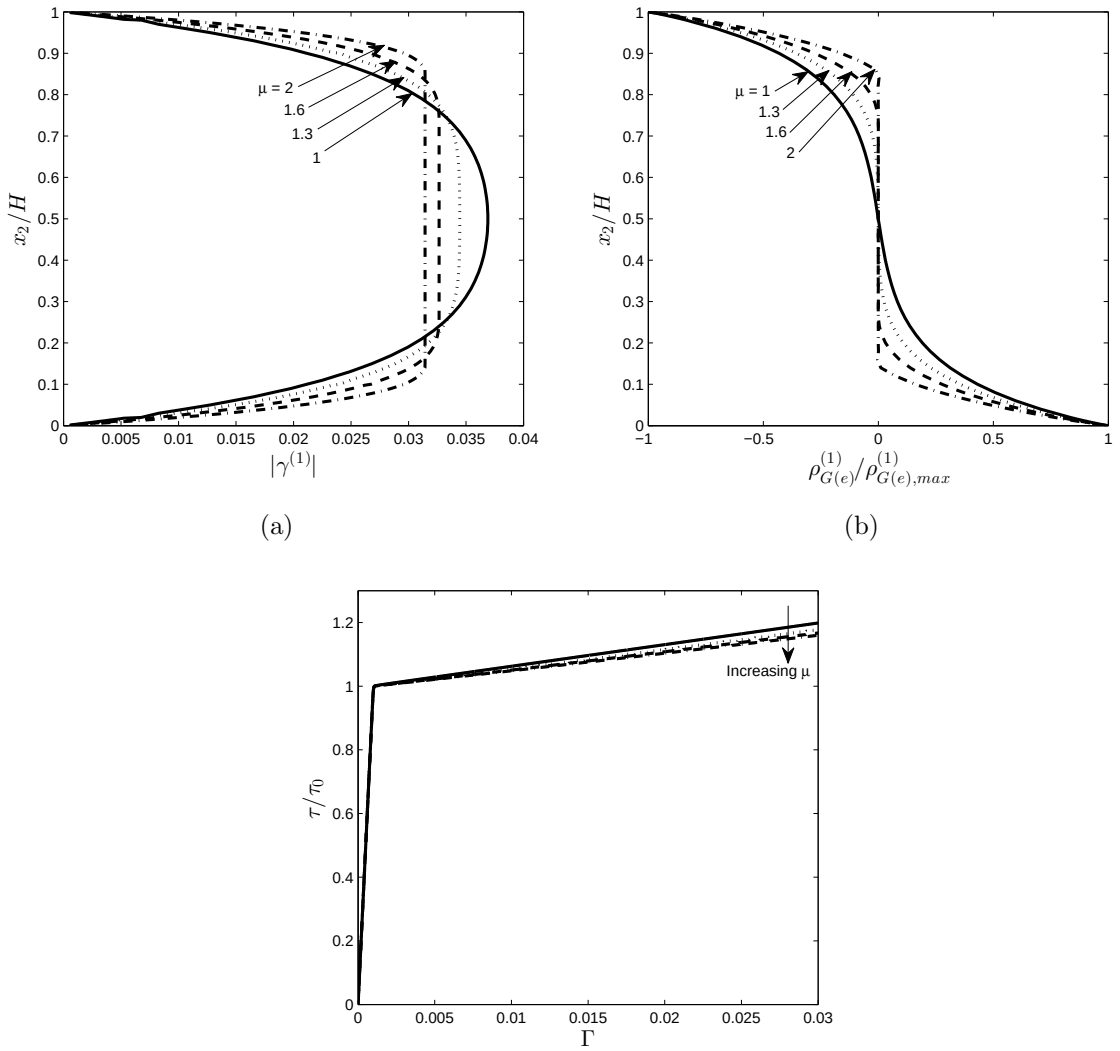

Figure 4: Numerical results for the single slip simple shear problem (Fig. 1), using the generalized gradient energy based back stress (Eqs. (19) and (20)), with $\theta = 90^\circ$ and $L/H = 0.3$, illustrating the effect of the μ parameter in the quadratic to cubic regime ($1 \leq \mu \leq 2$). The figure shows (a) slip profile, (b) normalized GND density, (c) shear stress vs. macroscopic shear strain.

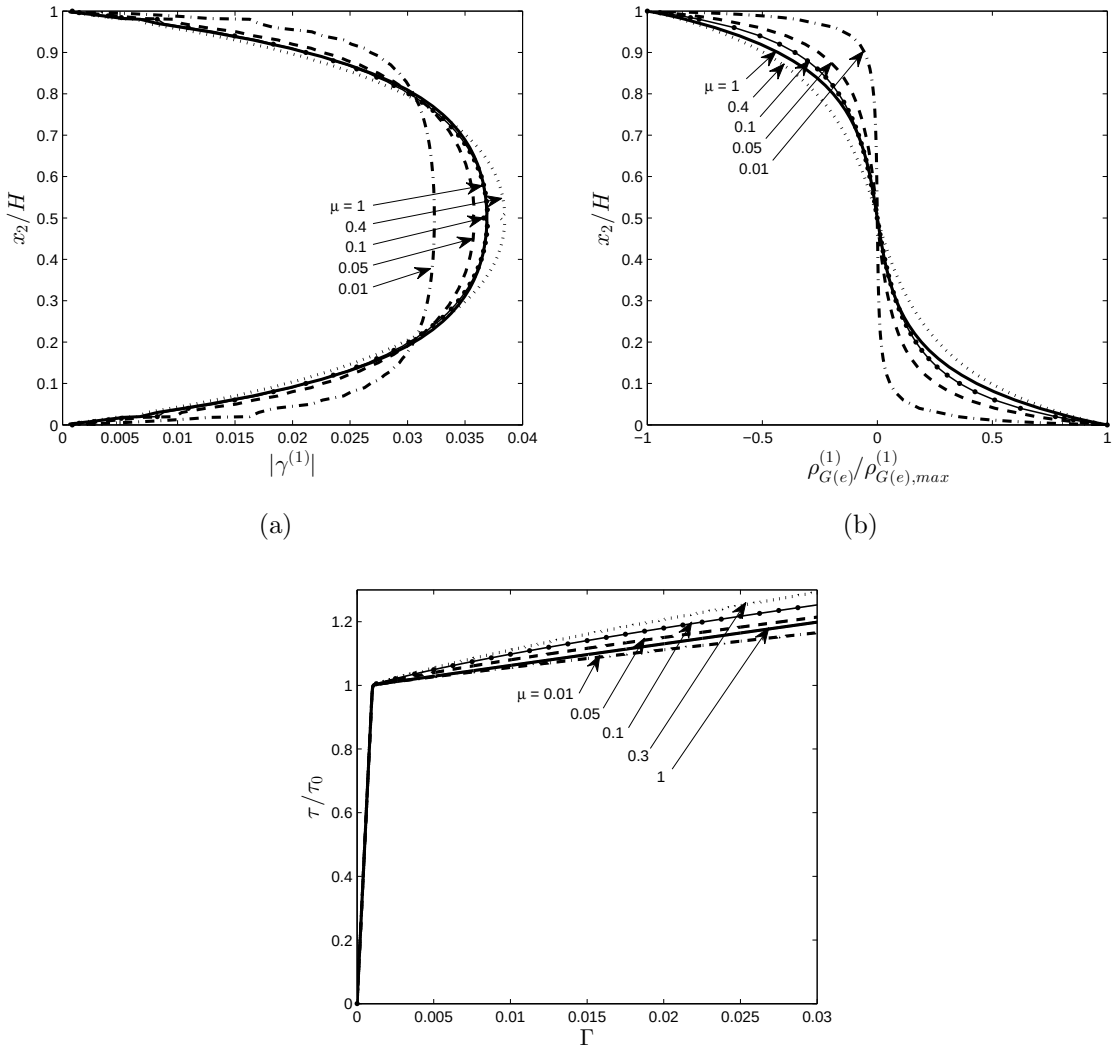

Figure 5: Numerical results for the single slip simple shear problem (Fig. 1), using the generalized gradient energy based back stress (Eqs. (19) and (20)), with $\theta = 90°$, $L/H = 0.3$, and $\rho_{G(e),0} = 10^5$ m^{-2}, illustrating the effect of the μ parameter in the linear to quadratic regime ($0 < \mu \leq 1$). The figure shows (a) Slip profile, (b) normalized GND density, and (c) shear stress vs. macroscopic shear strain.

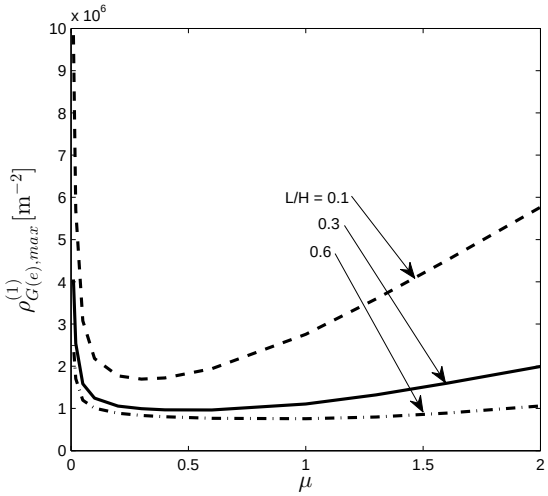

Figure 6: Magnitude (normalization values in Figs. 7b and 8b) of GND density as function of μ (Eqs. (19) and (20)) at a macroscopic shear strain of $\Gamma = 0.03$. Results are shown for different values of the material length scale parameter L.

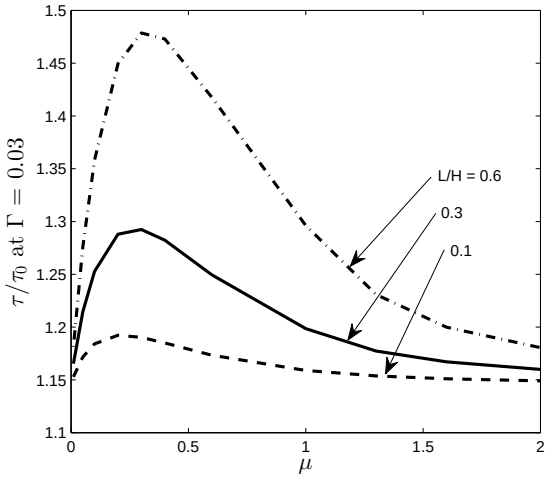

Figure 7: Shear flow stress at macroscopic shear strain $\Gamma = 0.03$ as function of μ, illustrating the effect of μ (Eqs. (19) and (20)) on the stress/strain response in Figs. 4c and 5c. Results are shown for different values of the material length scale parameter L

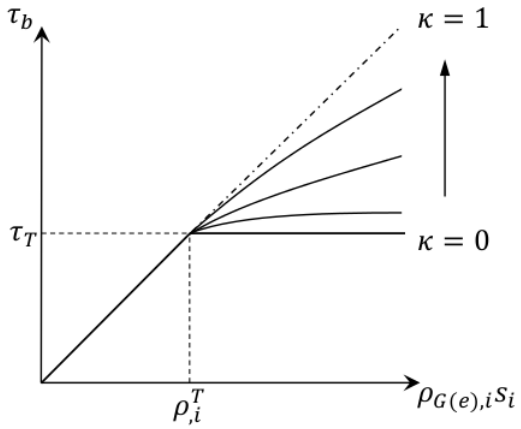

Figure 8: Schematic illustration of the back stress power law (Eq. 22).

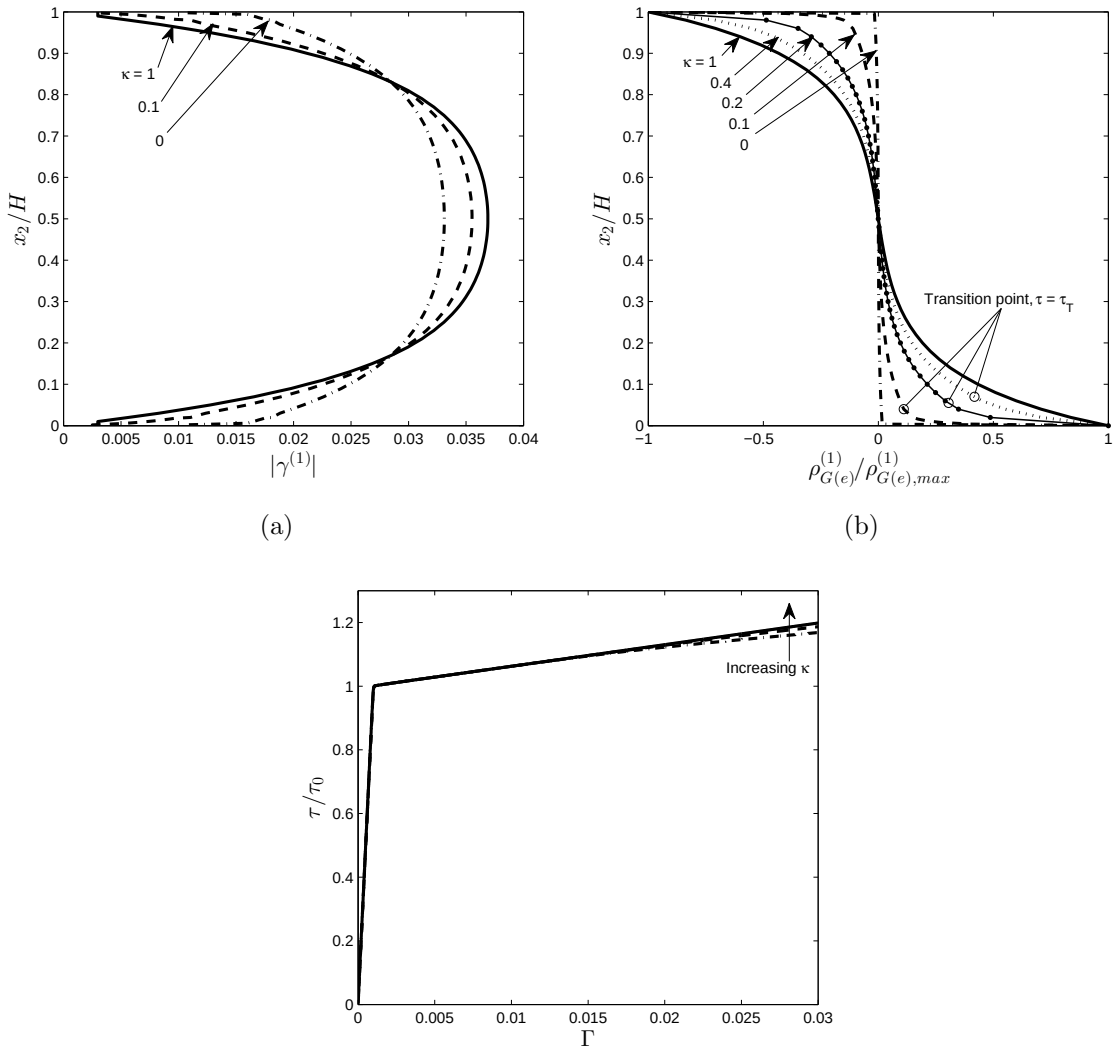

Figure 9: Numerical results for the single slip simple shear problem (Fig. 1), using the back stress power law (Eq. (22)), with $\theta = 90°$, $L/H = 0.3$, and $\tau_T/\tau_0 = 0.12$, illustrating the effect of the κ parameter. The figure shows (a) Slip profile, (b) normalized GND density, with circles marking the transition point $\tau_b = \tau_T$, and (c) shear stress vs. macroscopic shear strain.

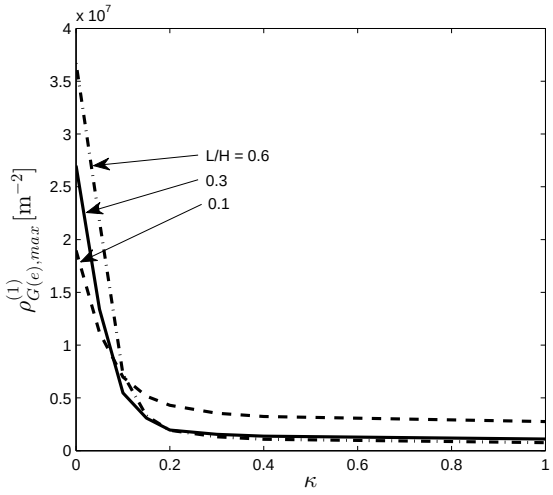

Figure 10: Magnitude (normalization values in Fig. 4b) of GND density as function of κ (Eq. 22) at a macroscopic shear strain of $\Gamma = 0.03$. Results are shown for different values of the material length scale parameter L

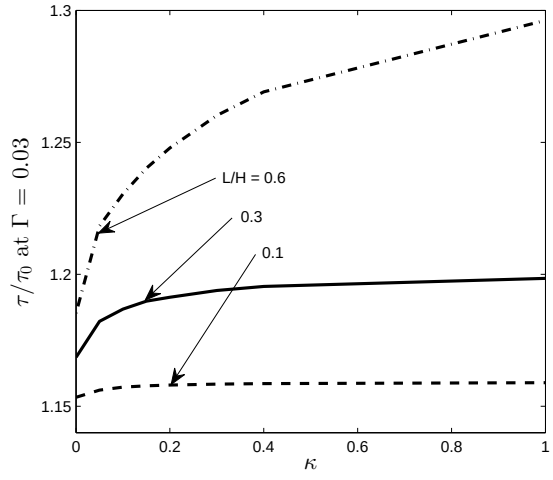

Figure 11: Shear flow stress at 0.03 macroscopic shear strain as function of κ (Eq. 22), to illustrate the effect of κ on the stress/strain response in Fig. 9c. Results are shown for different values of the material length scale parameter L

Appendix A. The effect of $\rho_{G(e),0}$

The GND density parameter value $\rho_{G(e),0} = 10^5$ m^{-2} was chosen for the computations in the present study in order to facilitate a solution for all used model parameters. The singularity of the back stress relation in Eq. (20) has an increasing effect as $\rho_{G(e),0}$ is decreased—rendering a solution impossible for very low values of $\rho_{G(e),0}$. Letting $\mu \longrightarrow 1$ further accentuates this effect, as μ also controls the extent of the singularity effect. In Fig. A.12, the effect of $\rho_{G(e),0}$ is demonstrated through a comparison of GND density at the microscopic hard boundary (See Fig. 1). For a material length scale of $L/H = 0.3$, results obtained with $\rho_{G(e),0} = 10^5$ m^{-2} are compared to results for $\rho_{G(e),0} = 10^4$ m^{-2}. It is seen that the effect of $\rho_{G(e),0}$ is most pronounced for the low intermediate values of μ.

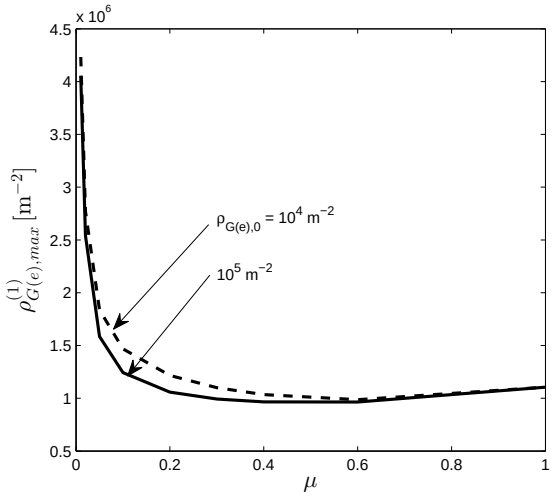

Figure A.12: Magnitude of GND density as function of μ (Eqs. (19) and (20)) at a macroscopic shear strain of $\Gamma = 0.03$ for $L/H = 0.3$. Results are shown for two different orders of magnitude of $\rho_{G(e),0}$.